New parton structure functions and minijets in the two-component dual parton model

F. W. Bopp and D. Pertermann
Fachbereich Physik, Universität Siegen, D-57068 Siegen, Federal Republic of Germany

R. Engel
Fachbereich Physik, Universität Leipzig, D-04109, Leipzig, Federal Republic of Germany

J. Ranft
INFN, Sezione di Milano, Via Celoria 16, I-20133 Milano, Italy
(Received 22 December 1993)

We use new fits to parton structure functions, including structure functions with Lipatov behavior at small x values and discuss the minijet component in the two-component dual parton model with a supercritical Pomeron as demanded by the fits to cross-section data. We find that a consistent model can only be formulated with a $p_{\perp\mathrm{hr}}$ cutoff for the minijets increasing with energy. The implications for particle production in hadronic collisions at TeV energies are discussed.

PACS number(s): 13.85.Hd, 12.39.−x, 12.40.Nn

I. INTRODUCTION

Soft multiparticle production characterizing hadronic interactions at high energies cannot be understood purely within theoretical approaches provided by perturbative QCD. The nonperturbative soft component of hadron production, which is responsible for all of hadron production at low energies is still acting at present and future collider energies.

Using the basic ideas of the dual topological unitarization scheme [1,2] the dual parton model (DPM) (a recent review is given in Ref. [3]) has been very successfully describing soft hadronic processes. Several new features of $p\bar{p}$ collisions at collider energies which were subsequently confirmed by experiments could be anticipated.

Observations such as rapidity plateaus and average transverse momenta rising with energy, Koba-Nielsen-Olesen (KNO) scaling violation, transverse momentum-multiplicity correlations and *minijets* pointed out that soft and hard processes are closely related. These properties were understood within the two-component dual parton model [4–9].

The hard component is introduced applying the lowest order of perturbative hard constituent scattering [10]. Single diffraction dissociation is represented by a triple-Pomeron exchange (high mass single diffraction) and a low mass component.

The Monte Carlo implementation of the dual parton model (DTUJET [5] for hadron-hadron collisions) enables us to investigate the predictions given by the model at energies of present and future hadron colliders. In the present paper we discuss mainly the minijet component. This is appropriate, since the first results from the DESY ep collider HERA on deep inelastic scattering at low x [11] seem to indicate that the structure functions at low x rise much stronger than anticipated in the past by most of the conventional structure function parameterizations. We will see that this, if also found for the gluon structure function, can lead to dramatic consequences for the minijet component.

In Sec. II we give a short account of the two-component dual parton model, in Sec. III we give details about the parton structure functions used to calculate the minijet cross sections, in Sec. IV we fit the parameters of the model to cross-section data, in Sec. V we investigate the multiparticle production in the resulting models, and in Sec. VI we give a summary.

II. THE TWO-COMPONENT DUAL PARTON MODEL

The soft input cross section in our unitarization scheme is described by the supercritical Pomeron

$$\sigma_s = g^2 s^{\alpha(0)-1} , \tag{1}$$

with g being the effective proton-Pomeron coupling constant and $\alpha(0)$ the Pomeron intercept. The corresponding Pomeron trajectory is given by $\alpha(t)=\alpha(0)+\alpha' t$. The supercritical Pomeron was used in the two-component DPM from the beginning [4], while other approaches use the critical Pomeron with $\alpha(0)=1$ from Durand and Pi [12] up to HIJING [13]. A large part of the differences between HIJING and the DPM results is due to this different starting point. In all fits of the Pomeron parameters to cross section data, including the ones we will report here, we get consistently better fits with the supercritical Pomeron than with the critical one.

These better fits to the supercritical Pomeron are one of our arguments for the continuous presence of the soft component to multiparticle production in the TeV energy region.

Furthermore we introduce graphs with Pomeron-Pomeron couplings. Provided that the Pomeron-Pomeron coupling constant Γ is small in comparison with other couplings, such as g, it is sufficient to consider the expansion in Γ only up to first order [5]. Thus a correction to the pure Pomeron exchange is represented by the triple-Pomeron graph [Fig. 1(c)] included with an

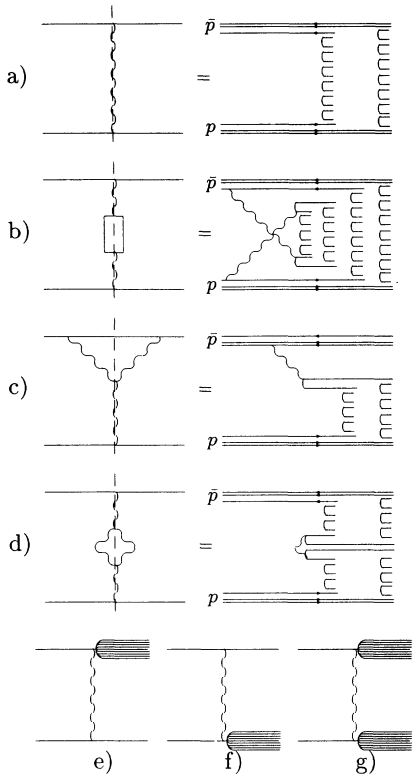

FIG. 1. Diagrams and the corresponding cut graphs for the exchange of (a) one soft Pomeron, (b) one hard Pomeron, and (c) one triple-Pomeron (high mass single diffraction). (d) shows one cut Pomeron-loop graph (high mass double diffraction). Low mass single diffractive processes (e), (f) and low mass double diffractive processes (g) are introduced via a two-channel eikonal formalism.

input cross section:

$$\sigma_{\rm TP}=\frac{2}{16\pi}\frac{g^3\Gamma}{b_{\rm sd}}\ln\frac{s}{s_0}\ , \tag{2}$$

where b_{sd} is the slope $b_{sd}=b_{sd}^0+2\alpha'\ln(s), b_{sd}^0=3.7$ GeV^{-2}, $\alpha'=0.24$ GeV^{-2} and $s_0=100$ GeV^2. (The numbers given here are the ones used in the published model [5]; in Sec. IV we will determine these parameters for the model presented here in fits to cross-section data.) The simplest cut of the triple-Pomeron [Fig. 1(c)] corresponds to a high mass single diffractive interaction. High mass diffraction is a comparatively rare process. High mass means that the diffractively excited system should not be a well-defined hadron resonance. We also describe high mass double diffractive processes again to first-order introducing loop graphs [Fig. 1(d)], with a cross section

$$\sigma_L=\frac{1}{16\pi}\frac{g^2\Gamma^2}{2b_{\rm DD}}\left[\ln^2\frac{s}{s_0}+\ln^2\frac{s_0'}{s}-2\ln^2\frac{5}{20}\right] \tag{3}$$

with $b_{\rm DD}$ being the slope parameter $b_{\rm DD}=2\alpha'\ln(s), s_0=400$ GeV^2, and $s_0'=25$ GeV^2.

The input cross section for semihard multiparticle production σ_h is calculated applying the QCD improved parton model as described in Refs. [4,7,8,14]:

$$\sigma_h=\sum_{i,j}\int_0^1 dx_1\int_0^1 dx_2\int d\hat{t}\frac{1}{1+\delta_{ij}}\frac{d\sigma_{{\rm QCD},ij}}{d\hat{t}} \times f_i(x_1,Q^2)f_j(x_2,Q^2) \times\Theta(p_\perp-p_{\perp{\rm thr}})\ , \tag{4}$$

$f_i(x,Q^2)$ are the structure functions of partons with the flavor i and scale Q^2 and the sum i,j runs over all possible flavors. To remain in the region where perturbation theory is valid, we use a low $p_\perp$ cutoff $p_{\perp{\rm thr}}$ for the minijet component. Furthermore, since we calculate $\sigma_{{\rm QCD},ij}$ in lowest-order QCD perturbation theory we multiply the hard input cross section σ_h with a K factor in the range of 1.5 to 2. A hard interaction leads to a chain system shown in Fig. 1(b).

The momentum fractions of the constituents at the ends of the different chains are sampled using the exclusive parton distribution, which has the form, for an event with n_s soft and $n_h(n_h\geq 1)$ hard Pomerons,

$$\rho(x_1,\ldots,x_{2n_s},\ldots,x_{2n_s+2+n_h})\sim\frac{1}{\sqrt{x_1}}\left[\prod_{i=3}^{2n_s+2}\frac{1}{x_i}\right]x_2^{1.5}\prod_{i=2n_s+3}^{2n_s+2+n_h}g(x_i,Q_i)\delta\left[1-\sum_{i=1}^{2n_s+2+n_h}x_i\right]. \tag{5}$$

The distributions $g(x_i,Q_i)$ are the distribution functions of the partons engaged in the hard scattering.

Soft(s), hard(h), high mass single diffractive(TP), and high mass double diffractive(L) processes are treated simultaneously within an eikonal unitarization scheme using the impact parameter representation

$$\chi_i(B,s)=\frac{\sigma_i(s)}{8\pi b_i}\exp\left[-\frac{B^2}{4b_i}\right],\quad i=s,h,{\rm TP},L \tag{6}$$

normalized by

$$\int 2\chi_i(B,s)d^2B=\sigma_i \tag{7}$$

with b_h energy independent, $b_s=b_{\rm TP}=b_L=b+\alpha'\ln(s)$. The exclusive cross section for l_c cut soft Pomerons, m_c cut hard Pomerons, n_c cut triple-Pomeron graphs and p_c cut loop graphs is given by

$$\sigma(l_c,m_c,n_c,p_c,B,s)=\frac{(2\chi_s)^{l_c}}{l_c!}\frac{(2\chi_h)^{m_c}}{m_c!}\frac{(-2\chi_{\rm TP})^{n_c}}{n_c!} \times\frac{(-2\chi_L)^{p_c}}{p_c!}\exp[-2\chi(B,s)] \tag{8}$$

with

$$\chi(B,s)=\chi_s(B,s)+\chi_h(B,s)-\chi_{\rm TP}(B,s)-\chi_L(B,s)\ . \quad (9)$$

The total and elastic cross sections are given by

$$\sigma_{\rm tot}=4\pi\int_0^\infty BdB(1-\exp[\chi(B,s)])\ ,$$
$$\sigma_{\rm el}(B,s)=\tfrac{1}{4}[\sigma_{\rm tot}(B,s)]^2\ . \quad (10)$$

Diffractive processes characterized by the excitation of an initial hadron to intermediate resonances (low mass diffractive interactions) are introduced via a two channel eikonal formalism. As suggested in Ref. [5] a new coupling λ modifies the three graphs given in Figs. 1(e)–(g) and leads to a modification of each graph with l soft, m hard, n triple-Pomeron, and p loop exchanges.

The low mass (LMSD) and high mass (HMSD) single diffractive cross sections are given [5] by (the definitions for the $\sigma^{(i)}$ and $\chi^{(i)}$ are given in Ref. [5]).

$$\sigma_{\rm LMSD}(B,s)=\frac{1}{8}(\exp[-\chi^{(1)}(B,s)]-\exp[-\chi^{(2)}(B,s)])^2\ , \quad (11)$$

$$\tilde{\sigma}_{\rm HMSD}(B,s)=\frac{1}{4}\sum_{i=1}^{4}\tilde{\sigma}^{(i)}_{\rm HMSD}=\frac{1}{4}\sum_{i=1}^{4}(\exp[\chi^{(i)}_{\rm TP}(B,s)]-1)\exp[-2\chi^{(i)}(B,s)] \quad (12)$$

with $\tilde{\sigma}_{\rm HMSD}=\sigma_{\rm HMSD}+\sigma_{\rm HMLMSD}$ (high mass-low mass single diffraction).

III. CURRENT PARAMETRIZATIONS OF PARTON STRUCTURE FUNCTIONS

During 1992 and 1993 new data on deep inelastic scattering and new fits to parton structure functions were reported. New features of these fits include (i) the flavor dependence of sea quark distributions and (ii) a stronger rise of the structure functions at low x values, that is, in the region important for minijets. These fits by Martin, Roberts, and Stirling (MRS) [15] and by the CTEQ Collaboration [16] include functions with a conventional $1/x$ singularity of sea quark and gluon distributions (for instance, the MRS set D0 functions) as well as functions with a $1/x^{1.5}$ singularity (for instance the MRS set D− functions). The pre-HERA measurements do not allow us to decide between these two possibilities. However, there are theoretical arguments in favor of the $1/x^{1.5}$ singularity [17]. These more singular parton distributions were in the past used to calculate the minijets [7,8], but not taken very seriously. This has to be changed, since the first HERA data seem to favor just these singular parton distribution functions [11].

Gluons are the most important source of minijets; unfortunately, so far no HERA data for the gluon distributions are available, but we should start now to discuss the implementation of the more singular functions for minijets.

IV. DETERMINING THE FREE PARAMETERS OF THE MODEL IN FITS TO CROSS-SECTION DATA

A. DTUJET92, energy-independent cutoff $p_{\perp,\rm thr}$

We describe these fits and the resulting model (similar fits were already reported in [7,8]) without much detail. As in the past, we use two different cutoffs for the minijets $p_{\perp\rm thr}=2$ and 3 GeV/c. In Tables I and II we give the results of the fit, that are the optimal model parameters determined. In the fits we use the new structure function sets MRS set D0 and MRS set D− [15] and the corresponding CTEQ functions [16]. Using the MRS structure functions we use the scale $Q^2=p_\perp^2/4$ as in our previous papers, but in the case of the CTEQ structure functions we chose a different scale $Q^2=p_\perp^2$. This different choice is required in order to remain in the Q^2 range of the parametrizations. For all considered parton distributions we obtained acceptable fits and acceptable descriptions of the data. In Figs. 2 and 3 for the MRS structure functions and in Figs. 4 and 5 for the CTEQ structure functions we compare the calculated cross sections to the data from the CERN Intersecting Storage Rings (ISR) to Fermilab Tevatron energies. The data for total and elastic cross sections used in the fits and plotted in Figs. 2 and 4 and later figures are from Refs. [18–23]. The data for diffractive cross sections used in the fits and plotted in Figs. 3 and 5 and later figures are from Refs. [23–29]. Not used in the fits but included in the plots are cosmic ray data [30,31]. The fit results (see Tables I and II) show that $\alpha(0)$ always corresponds to a supercritical soft Pomeron. Because of the uncertainties of the parton distributions at low x values the extrapolation already of all these cross sections to high energies is rather difficult. We are not able to give a unique prediction of the behavior of the cross sections at supercollider energies. The reason for this is the input minijet cross sections, which we calculate using the two different parton distributions: We obtain at $\sqrt{s}=40$ TeV approximately with MRS set D0 $\sigma_h=200$ mb and with MRS set D− $\sigma_h=1200$ mb. The unitarization method compensates for most of the difference and gives output values of $\sigma_{\rm tot}$ of about 120 and 160 mb, respectively. If we calculate the rapidity distributions in the two models the differences are much bigger. In Fig. 6 we plot pseudorapidity distributions obtained using the MRS set D0 structure functions and compare to experimental data. In Fig. 7 we plot the central pseudorapidity plateau as a function

TABLE I. Model parameters obtained with a $p_{\perp\rm thr}$ of 3 GeV/c. In the last column the χ^2 values divided by the degrees of freedom (DF) are listed.

PDF set	g^2(mb)	$\alpha(0)$	λ	$\chi^2/N_{\rm DF}$
MRS set D0	52.9±1.3	1.073±0.003	0.73±0.02	5.5
MRS set D−	54.4±1.4	1.069±0.003	0.72±0.02	4.8
CTEQ set 1M	52.4±1.3	1.074±0.002	0.74±0.02	5.0
CTEQ set 1MS	52.4±1.4	1.074±0.002	0.74±0.02	4.9
CTEQ set 1ML	53.3±1.3	1.072±0.003	0.73±0.02	4.6
CTEQ set 1L	51.8±1.4	1.076±0.002	0.74±0.02	5.1

TABLE II. Model parameters obtained with a $p_{\perp thr}$ of 2 GeV/c. In the last column the χ^2 values divided by the degrees of freedom (DF) are listed.

PDF set	g^2(mb)	$\alpha(0)$	λ	χ^2/N_{DF}
MRS set D0	68.5±1.0	1.029±0.002	0.58±0.01	1.1
MRS set D−	63.1±1.1	1.049±0.002	0.68±0.02	3.2
CTEQ set 1M	60.8±1.2	1.051±0.003	0.67±0.03	2.1
CTEQ set 1MS	61.3±1.1	1.053±0.003	0.67±0.02	2.1
CTEQ set 1ML	64.5±1.3	1.042±0.002	0.64±0.02	1.4
CTEQ set 1L	57.2±1.4	1.060±0.003	0.70±0.02	3.1

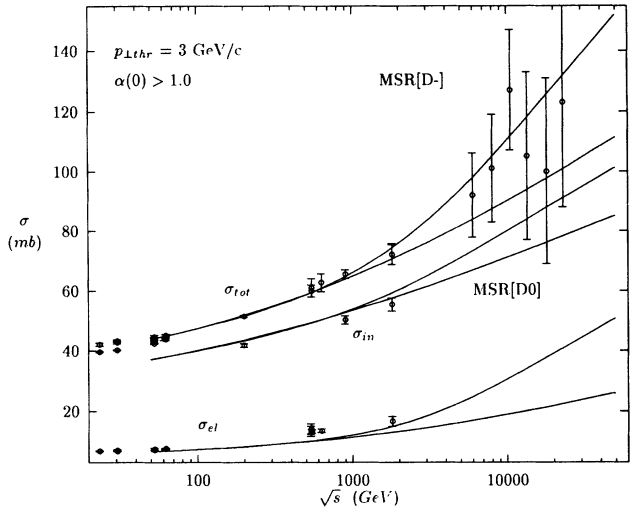

FIG. 2. Cross sections σ_{tot}, σ_{el}, and σ_{inel} calculated using the MRS structure functions, compared with the two-component DPM DTUJET92.

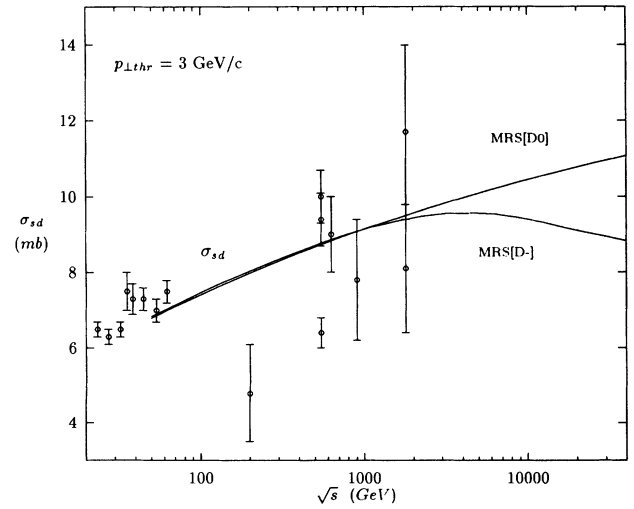

FIG. 3. Cross section σ_{diff} calculated using the MRS structure functions, compared with the two-component DPM DTUJET92.

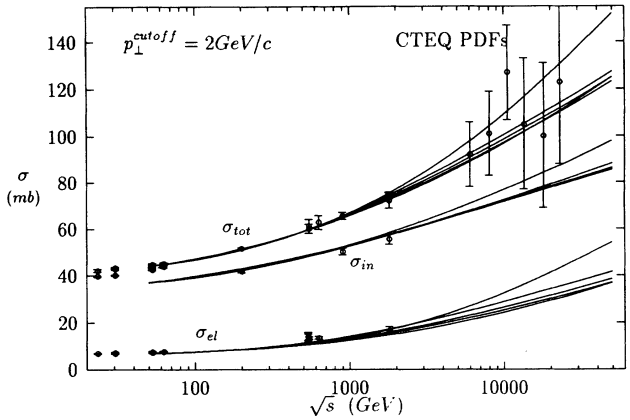

FIG. 4. Cross sections σ_{tot}, σ_{el}, and σ_{inel} calculated using the CTEQ structure functions, compared with the two-component DPM DTUJET92.

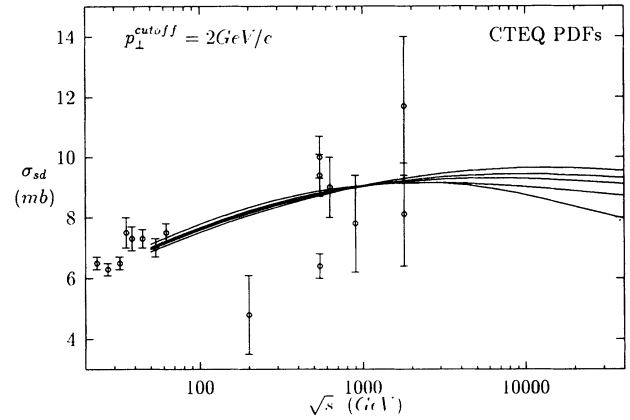

FIG. 5. Cross section σ_{diff} calculated using the CTEQ structure functions, compared with the two-component DPM DTUJET92.

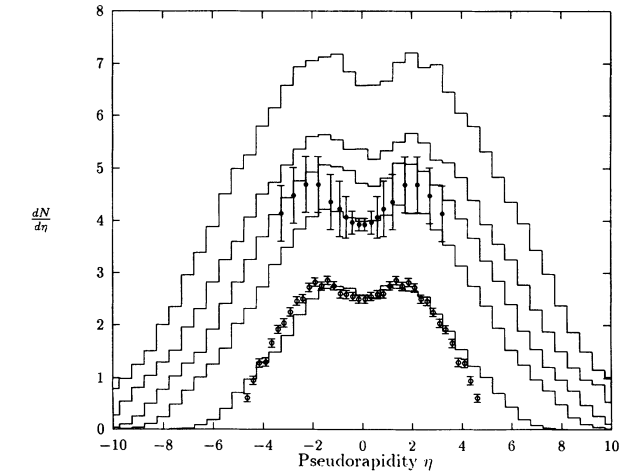

FIG. 6. Pseudorapidity distributions in DTUJET92 with MRS set D0, compared to collider data [37,38] and extrapolated to TeV energies. From top to bottom the energies are: $\sqrt{s}$ =40, 14.6, 5, 1.8, and 0.2 TeV.

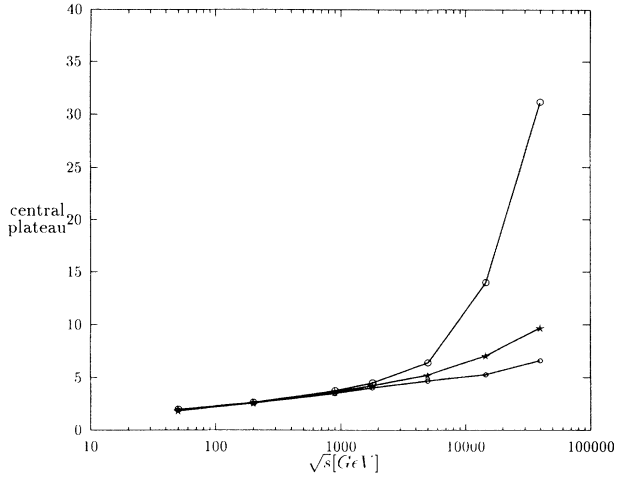

FIG. 7. Rise of the pseudorapidity plateau in DTUJET92. The three curver are, from top to bottom, calculated with the structure functions MRS set D−, CTEQ set 1ML and MRS set D0.

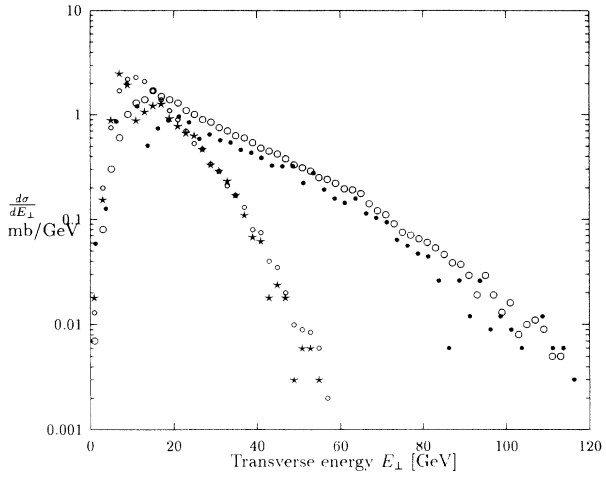

FIG. 9. Comparison of transverse energy distributions with collider data [39]. Open symbols: experimental data, solid symbols: DTUJET92. Upper curves: $\sqrt{s}=900$ GeV, lower curves: $\sqrt{s}=200$ GeV.

of the energy for the two models; up to present collider energies both models agree with each other and with the experimental data but in the supercollider energy region the differences are very big.

At present CERN and Tevatron collider energies, there is nothing wrong with this model and indeed, DTUJET92, with JETSET [32] fragmentation and parton evolution gives with all MRS and CTEQ parton distribution functions (PDF's) an excellent phenomenology. See Fig. 6, where we compare with pseudorapidity distributions, Fig. 8, where we compare with transverse momentum distributions, Fig. 9, where we compare with transverse energy distributions or Fig. 10, where we compare with average transverse momentum—multiplicity correlations for produced pions and antiprotons.

At these energies the model is still consistent, since the minijet cross sections are small.

In Fig. 7 we plot the rise of the pseudorapidity plateau in this model with different structure functions. We see, extrapolating with MRS set D− into the tens of TeV energy region, the model becomes inconsistent and produces unreliable results such as a pseudorapidity plateau at the energy of 40 TeV of 30–35 charged hadrons per pseudorapidity unit, while previous versions of the model and the same model with conventional PDF's give plateaus between 6 and 8 charged particles per pseudorapidity unit.

At these energies and with MRS set D− structure function the DTUJET92 *model has become inconsistent and is wrong.*

What is inconsistent and wrong? The input minijet

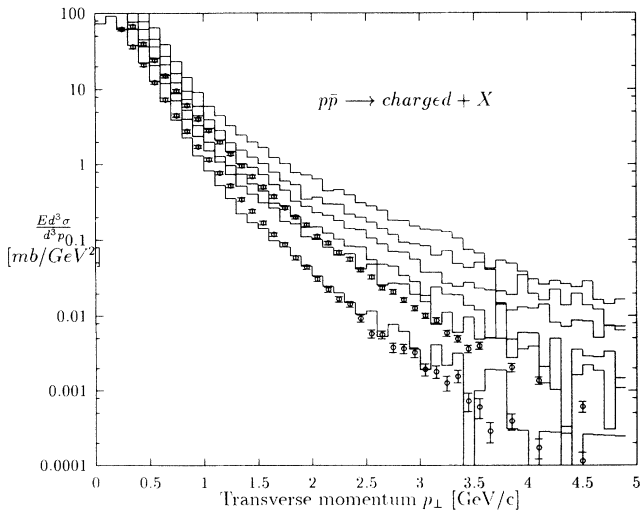

FIG. 8. Comparison of transverse momentum distributions with collider data [39]. The calculation uses the structure function CTEQ set 1ML. The energies are from top to bottom: $\sqrt{s}=40$, 14.6, 5, 1.8, 0.9 and 0.2 TeV.

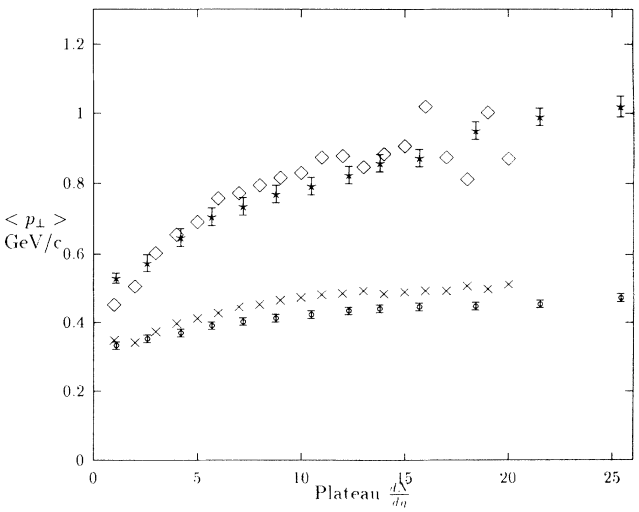

FIG. 10. Comparison of average transverse momentum—multiplicity correlations with collider data [41]. The calculated values are without, the experimental data are with error-bars.

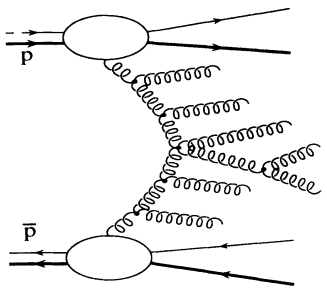

FIG. 11. A typical process, where n minijets are produced.

cross section σ_h, which we put so far into the unitarization scheme, are inclusive cross sections normalized to $n_{\text{minijets}}\sigma_{\text{inel}}$, where n_{minijets} is the multiplicity of minijets. But the physical processes, which contribute to this inclusive cross section, if we use parton distributions with Lipatov behavior, are $2\rightarrow n$ parton processes. In Fig. 11 we give such a typical process. $2\rightarrow n$ processes give a contribution to σ_h equal to $n\sigma_{2\rightarrow n}$. Furthermore, the s-channel iteration of such a huge cross section is probably incorrect. If we treat this huge cross section as σ_h in the usual way in the eikonal unitarization scheme we replace it by $n/2$ simultaneous $2\rightarrow 2$ parton processes such as the one given in Fig. 12; this is the inconsistency. What we should really use in the unitarization, but what we do not know how to compute reliably at present, would be

$$\sigma_h = \sum_n \sigma_{2\rightarrow n} \tag{13}$$

B. DTUJET93, energy-dependent cutoff $p_{\perp,\text{thr}}$

The way to remove this inconsistency is to make in DTUJET93 the threshold for minijet production $p_{\perp\text{thr}}$ energy dependent in such a way that at no energy and for no PDF is the resulting σ_h bigger than the total cross section. Then at least we have a cross section, which is indeed mainly the cross section of a $2\rightarrow 2$ parton process at this level, but we can get back to the real $2\rightarrow n$ processes via parton showering. One possible form for this energy-dependent cutoff is

$$p_{\perp\text{thr}} = 2.5 + 0.12[\log_{10}(\sqrt{s}/\sqrt{s_0})]^3 \ \ [\text{GeV}/c] \ , \qquad \sqrt{s_0} = 50 \text{ GeV} \ . \tag{14}$$

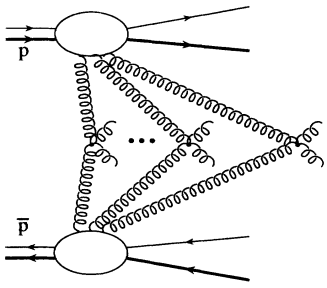

FIG. 12. The eikonalization gives n simultaneous $2\rightarrow 2$ parton processes.

The resulting σ_h are smaller than the total cross sections resulting after the unitarization for all MRS and CTEQ PDF's and also the older Kwiecinski-MRS (KMRS) [33] distributions. We note that this energy dependent $p_\perp$ cutoff corresponds numerically closely to the one used by Geiger [34–36], but the physical motivation for its use is of course completely different.

Now we are again consistent. We use, as first described in [14] at $p_{\perp\text{thr}}$, the continuity requirement for the *soft* and *hard* chain end $p_\perp$ distributions. Physically, this means that we use the soft cross section to cut the singularity in the minijet $p_\perp$ distribution. But note that this cut moves with rising collision energy to higher and higher $p_\perp$ values. This procedure has, in addition to cutting the singularity, more attractive features.

(i) The model results (at least as long as we do not violate the consistency requirement described above) become largely independent from the otherwise arbitrary $p_\perp$ cutoff. This was already demonstrated with DTUJET90 [5] and cutoffs of 2 and 3 GeV/c. This property is also seen in the present paper; we need only to compare results obtained with conventional structure functions with DTUJET92 and DTUJET93, which differ drastically in the prescription for the $p_\perp$ cutoff.

(ii) The continuity between soft and semihard physics is emphasized; there is no basic difference between soft and semihard chains other than the technical problem that perturbative QCD allows only to calculate the semihard component.

(iii) With this continuity in mind we feel free to call all chain ends, whatever their origin in the model, minijets, as soon as their $p_\perp$ exceeds a certain value, say 2 GeV/c.

We turn now to the fit of the Pomeron parameters in the case of DTUJET93 with the energy dependent $p_\perp$ cutoff given above. To describe the high energy particle production we have to determine the free parameters of the model, i.e., the proton-Pomeron coupling constant g, the effective soft Pomeron intercept $\alpha(0)$, the slope of the Pomeron trajectory α', the slope parameters b and b_h, and the excitation coupling constant λ. This has been done by a global fit to all available data of total, elastic, inelastic, and single diffractive cross sections in the energy range from ISR to collider experiments as well as to the data on the elastic slopes in this energy range. Since there are large differences in the hard parton distribution functions at small x values resulting in different hard input cross sections we have to perform separate fits for each set of parton distribution functions.

We get again good fits using all of the PDF's, which also as before give us a supercritical Pomeron, not a critical one. In Table III we give the parameters obtained in the fit. All the values obtained for $\alpha(0)$ demonstrate again that the fits result in a supercritical Pomeron. In Figs. 13 and 14 we plot the fitted cross sections obtained with the MRS PDF's together with the data, in Figs. 15 and 16 the same is done for three of the CTEQ parton distributions. We note that the differences of the output σ_{tot} obtained with the conventional MRS set D0 and the Lipatov behaved MRS set D− structure functions are much smaller than in the fit with constant $p_{\perp\text{thr}}$.

In order to demonstrate the continuity of soft and sem-

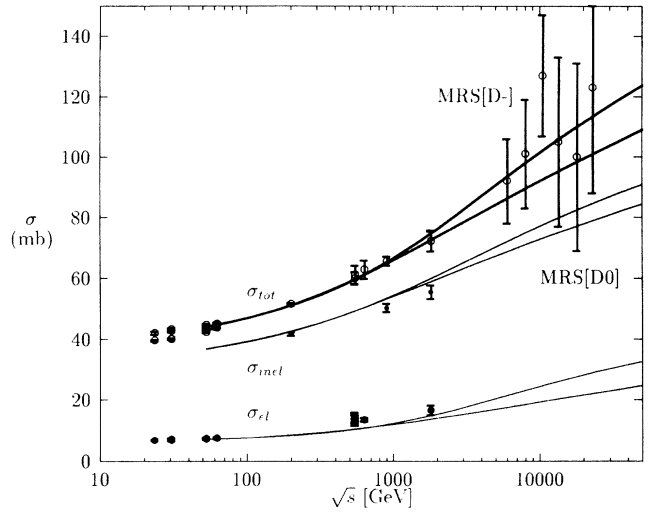

FIG. 13. Cross section σ_{tot},σ_{el}, and σ_{inel} compared with the two-component DPM DTUJET93. (MRS set D0 and MRS set D−).

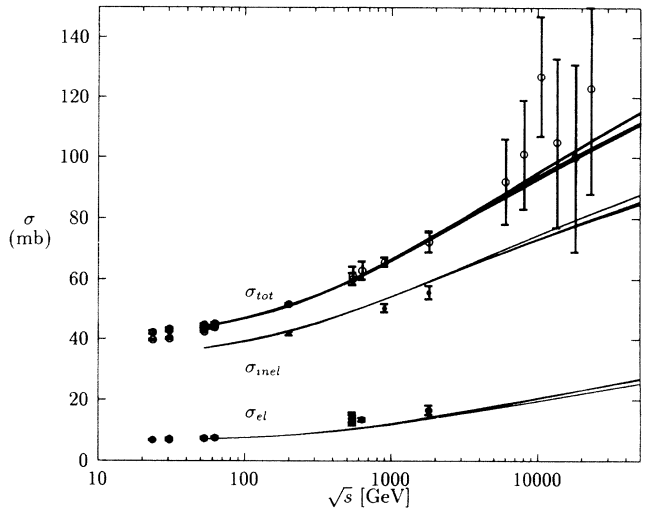

FIG. 15. Cross sections σ_{tot},σ_{el}, and σ_{inel} compared with two-component DPM DTUJET93 (CTEQ set 1M, CTEQ set 1MS, and CTEQ set 1ML).

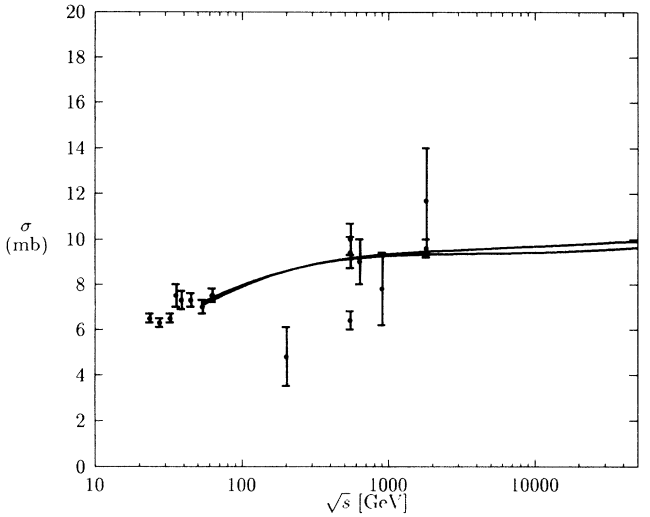

FIG. 14. Cross sections σ_{diff} compared with the two-component DPM DTUJET93 (MRS set D0 and MRS set D−).

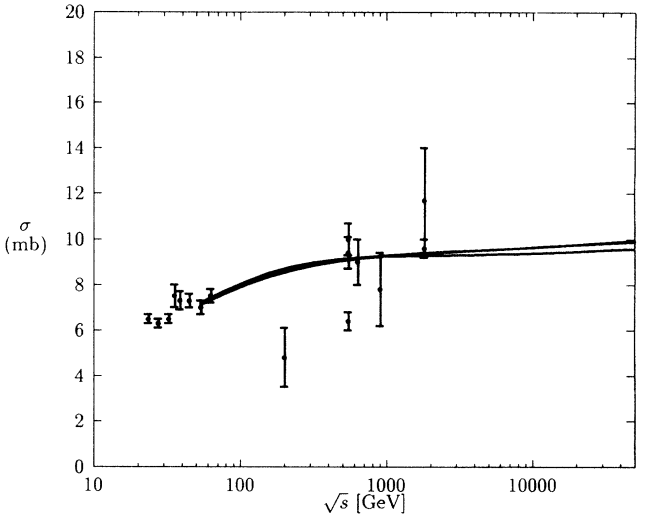

FIG. 16. Cross sections σ_{diff} compared with the two-component DPM DTUJET93 (CTEQ set 1M, CTEQ set 1MS, and CTEQ set 1ML).

TABLE III. DTUJET93 model parameters obtained with an energy dependent $p_{\perp\text{thr}}$.

PDF set	g^2(mb)	$\alpha(0)$	α' [GeV^{-2}]	b [GeV^{-2}]	b_h [GeV^{-2}]	λ
MRS set D0	49.14	1.0636	0.173	1.63	4.01	0.565
MRS set D−	55.96	1.0490	0.351	1.038	2.01	0.584
CTEQ set 1M	50.85	1.0589	0.210	1.516	3.44	0.562
CTEQ set 1MS	52.25	1.0560	0.256	1.365	2.96	0.574
CTEQ set 1ML	53.73	1.0489	0.250	1.390	2.83	0.529
CTEQ set 1DIS	49.85	1.0616	0.188	1.583	3.75	0.565
CTEQ set 1L	49.56	1.0614	0.208	1.520	3.81	0.593

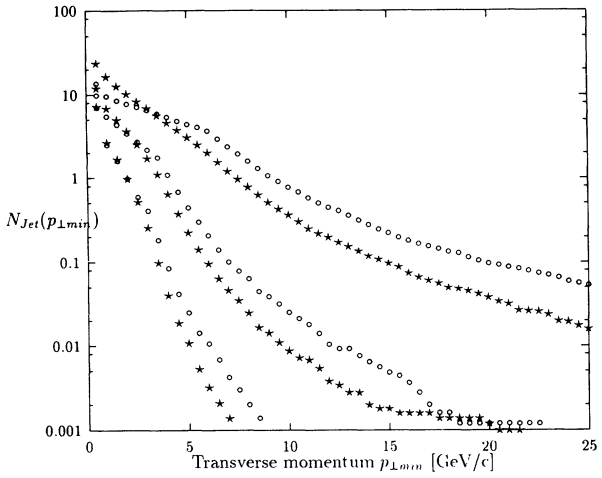

FIG. 17. Number of jets with $p_\perp \geq p_{\perp thr}$, DTUJET93 with CTEQ[1ML]. Open symbols: model without parton evolution, solid symbols: model with parton evolution. The energies for the three sets of curves are from top to bottom: $\sqrt{s}$ =40, 1.8, and 0.2 TeV.

ihard chain end $p_\perp$ distributions we plot in Figs. 17 and 18 always at three energies the numbers of chain ends with $p_\perp$ bigger than $p_{\perp thr}$ as function of $p_{\perp thr}$. The plots are given before and after the parton evolution. The curves refer to the models with the CTEQ set 1ML and the MRS set D− parton distributions.

We observe that at 0.2 and 1.8 TeV the distribution according to these two structure functions are nearly identical, at these energies we use the structure functions in x regions, where experimental data are available and all structure functions agree largely. While in the distributions before the final state parton evolution the structure at $p_\perp = p_{\perp thr}$ is always visible, the curves become rather smooth after the parton evolution. As to be expected, the parton evolution decreases the distributions at large $p_\perp$ values and increases the distributions at small $p_\perp$ values.

V. MULTIPARTICLE PRODUCTION WITH DTUJET93

We get again a good phenomenology with all the known results at the CERN and Tevatron collider.

In Fig. 19 we compare the pseudorapidity distributions obtained in the model with the MRS set D− parton distributions with data at collider energies [37,38] and give the extrapolation up to CERN Large Hadron Collider (LHC) energies and beyond. In Fig. 20 we give the same comparison using the model with the CTEQ set 1ML parton distributions. The agreement with the data is similar in both cases, while there are slight differences in the extrapolations into the TeV energy range. We did not attempt to determine the free parameters in the model; these are essentially some parameters in the fragmentation code; see below, to obtain an optimum agreement to the data.

In Fig. 21 we plot the central rapidity plateau (upper three curves) and central pseudorapidity plateau obtained with DTUJET93 and the PDF's MRS set D0 , MRS set D− and CTEQ set 1ML as a function of the collision energy $\sqrt{s}$. No striking differences are seen between the three models. In Fig. 22 we plot and compare to data the average transverse momenta [39] in the central rapidity region obtained with DTUJET93 and the same three PDF's. While all three models agree well with the collider data, we find significant differences in the extrapolation into the supercollider energy region: The average $p_\perp$ rises more strongly for the more singular parton distribution functions.

In Fig. 23 we compare the model with UA7 data [40] for π^0 production in the fragmentation region. This is the only fragmentation region data available in the collid-

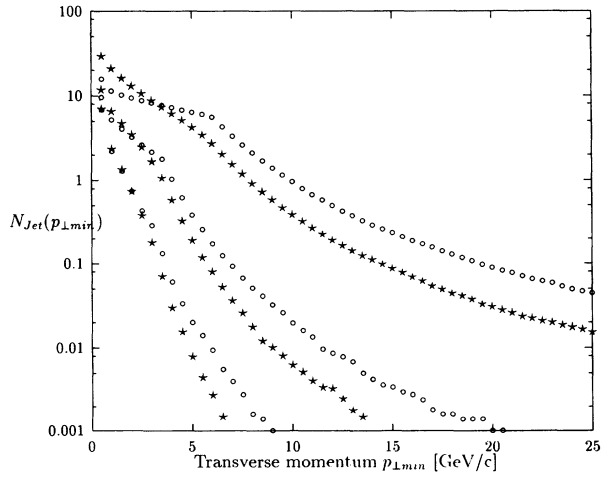

FIG. 18. Number of jets with $p_\perp \geq p_{\perp thr}$, DTUJET93 with MRS set D−. Open symbols: model without parton evolution, solid symbols: model with parton evolution. The energies for the three sets of curves are from top to bottom: $\sqrt{s}$ =40, 1.8, and 0.2 TeV.

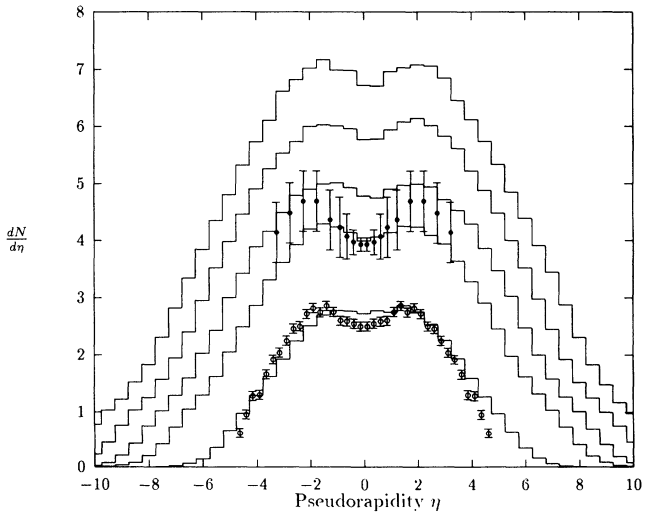

FIG. 19. Pseudorapidity distributions in DTUJET93 with MRS set D−, compared to collider data [37,38] and extrapolated to TeV energies. From top to bottom the energies are: $\sqrt{s}$ =40, 14.6, 5, 1.8 and 0.2 TeV.

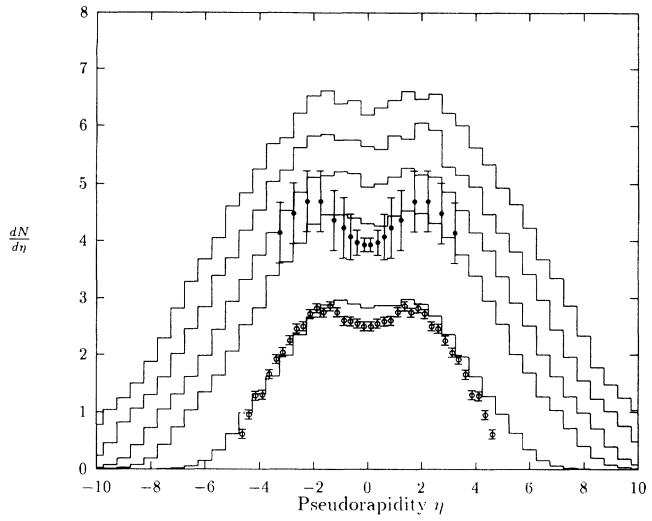

FIG. 20. Pseudorapidity distributions in DTUJET93 with CTEQ[1ML], compared to collider data [37,38] and extrapolated to TeV energies. From top to bottom the energies are: $\sqrt{s}$ =40, 14.6, 5, 1.8 and 0.2 TeV.

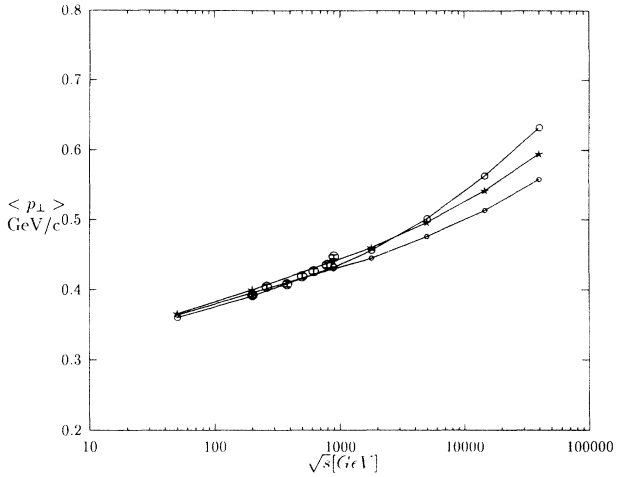

FIG. 22. The rise of central average transverse momenta with energy in several DTUJET93 models, data from [39]. Upper curve: MRS set D−, middle curve: CTEQ[1ML], lower curve: MRS set D0.

er energy range. The agreement with the data is similar in all versions of the model.

In Figs. 24 and 25 we compare transverse momentum distributions calculated with the models with the CTEQ set 1ML and MRS set D− parton distributions with UA1 data [39]. The agreement is satisfactory; the model gives the correct transition between the exponential falloff of the distributions at small $p_\perp$ to the power law falloff at larger $p_\perp$.

In Figs. 26 and 27 we compare transverse energy distributions calculated with the same two parton distributions with UA1 data [39], and we find again a reasonable agreement. These distributions are very similar to multiplicity distributions, since the average transverse momentum per produced hadron does not change much from one energy to another.

In Fig. 28 we compare $\langle p_\perp \rangle$ multiplicity correlations with data from the Tevatron collider [41], we get good agreement for pions and also for and antiprotons, for antiprotons the average transverse momenta rise much more strongly with multiplicity than for pions. The model is DTUJET93 with the MRS set D− parton distribution function.

In Figs. 29–31 we compare the DTUJET92 and DTUJET93 models with the CTEQ set 1ML parton distributions with the C_2, C_3, and C_4 multiplicity moments as measured by the UA5 Collaboration [42,43]. These multiplicity moments,

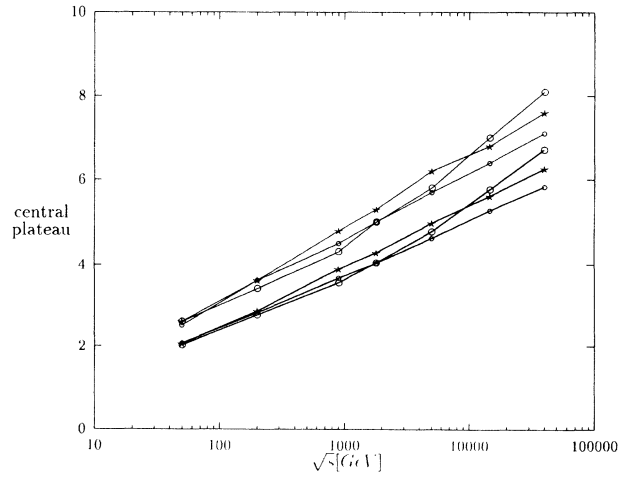

FIG. 21. The rise of the central rapidity (upper three curves) and pseudorapidity (lower three curves) plateau with energy in different DTUJET93 models (MRS set D−, MRS set D0 and CTEQ set 1ML).

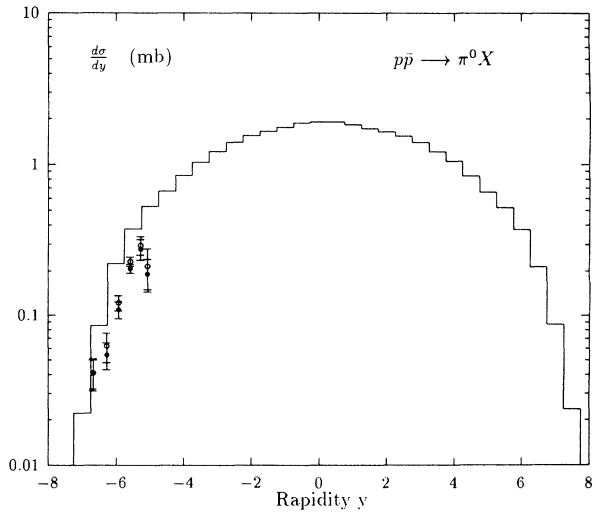

FIG. 23. Rapidity distribution of π^0 in the fragmentation region in DTUJET93 with MRS set D−, compared to collider data [40].

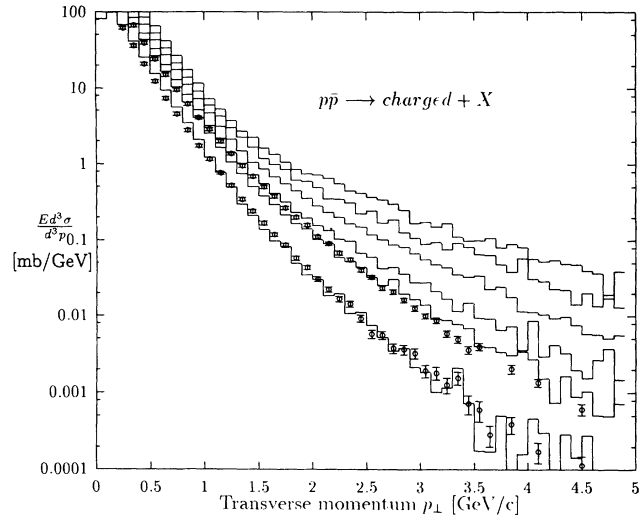

FIG. 24. Comparison of transverse momentum distributions with collider data [39]. The energies are from top to bottom: $\sqrt{s}=40$, 14.6, 5, 1.8, 0.9, and 0.2 TeV. The calculation uses the structure function CTEQ set 1ML.

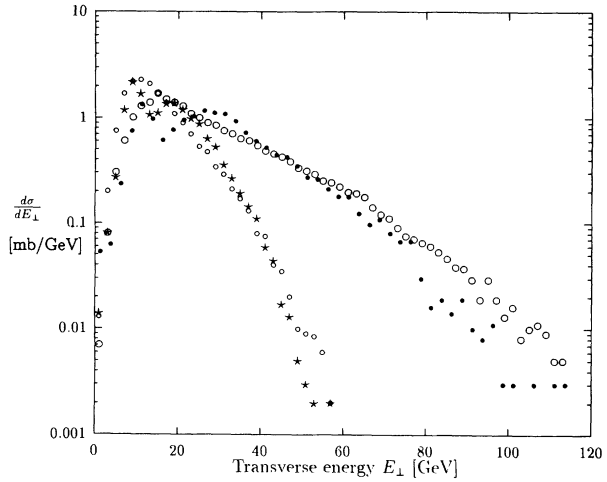

FIG. 26. Comparison of transverse energy distribution with collider data [39]. Open symbols: experimental data, solid symbols: DTUJET93. Upper curves: $\sqrt{s}=900$ GeV, lower curves: $\sqrt{s}=200$ GeV. The calculation uses the structure function CTEQ set 1ML.

$$C_n=\frac{\langle N^n\rangle}{\langle N\rangle^n}\ , \tag{15}$$

if not energy independent, are an indication for the violation of the KNO-scaling behavior of the multiplicity distributions.

All distributions presented in this paper have been obtained using the Lund code JETSET−7.3 [32] for the fragmentation of the strings. In the energy range considered, the parameters of JETSET are energy independent, but the best agreement to data is obtained with parameters differing slightly in DTUJET92 and DTUJET93. (For nondiffractive events in DTUJET92:PARJ(42)=3, PARJ(21)=0.37. For nondiffractive events in DTUJET93:PARJ(42)=1.8, PARJ(21)=0.45, for all other parameters we use the default parameters).

We conclude this section. Extrapolating to LHC energies, we get charged plateaus of 5–6 particles per pseudorapidity unit for the models with all MRS and CTEQ PDF's. However, the average transverse momenta in the models with the singular PDF's rise more steeply with energy than in previously published versions of DTUJET. We find using DTUJET93 at LHC energies an average $p_\perp$ typically 100 MeV/c bigger than previously.

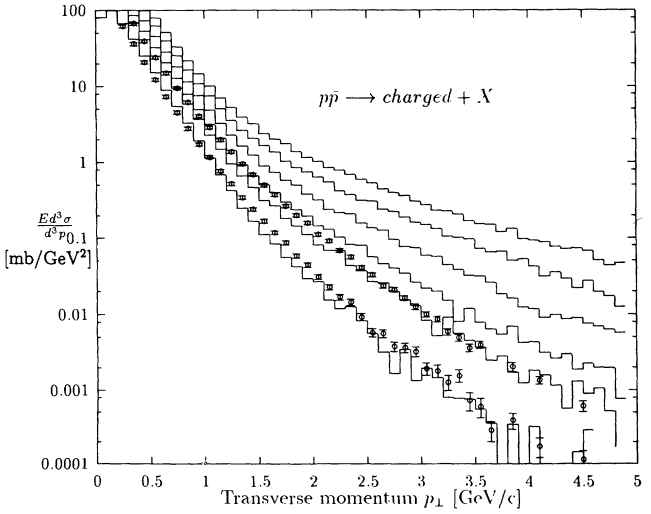

FIG. 25. Comparison of transverse momentum distributions with collider data [39]. The energies are from top to bottom: $\sqrt{s}=40$, 14.6, 5, 1.8, 0.9, and 0.2 TeV. The calculation uses the structure function MRS set D−.

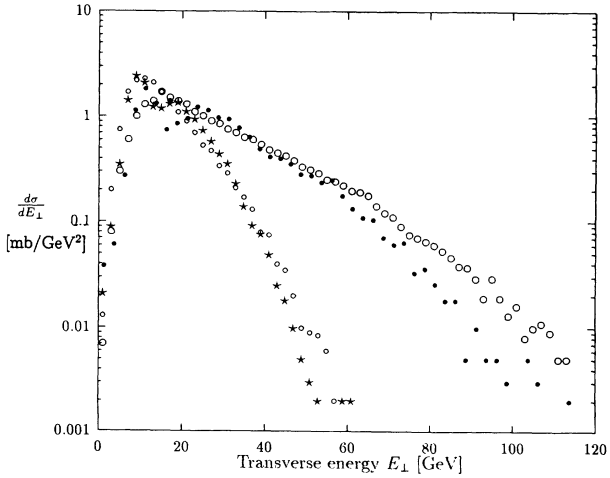

FIG. 27. Comparison of transverse energy distribution with collider data [39]. Open symbols: experimental data, solid symbols: DTUJET93. Upper curves: $\sqrt{s}=900$ GeV, lower curves: $\sqrt{s}=200$ GeV. The calculation uses the structure function MRS set D−.

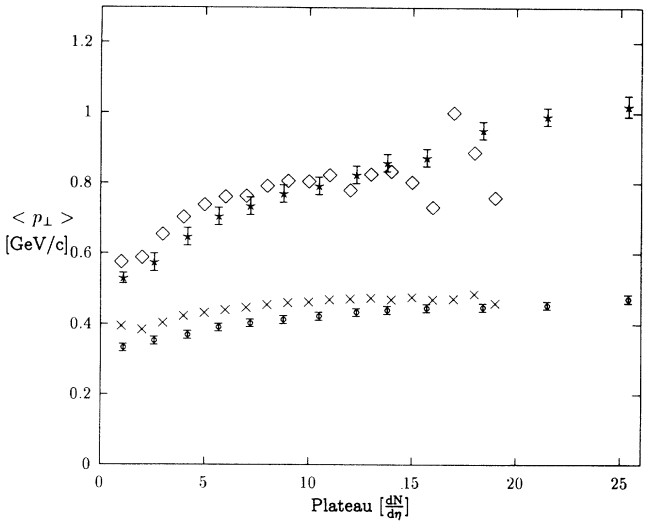

FIG. 28. Comparison of average transverse momentum—multiplicity correlations with collider data [41]. The calculated values are without, the experimental data are with error-bars.

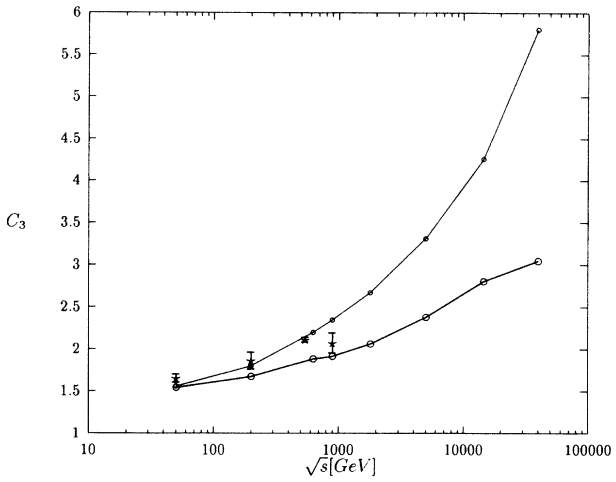

FIG. 30. Comparison of multiplicity moments with collider data [42,43]. The experimental data are with error bars, the upper curve is calculated with DTUJET92, the lower curve is calculated with DTUJET93.

VI. CONCLUSIONS AND SUMMARY

The two-component dual parton model has some natural way to cutoff the singularity of the minijet cross section at low $p_\perp$. The model uses the soft Pomeron cross section as the low $p_\perp$ limit of the minijets.

With the new prescription in DTUJET93 we find the plateau rising like ln$s$ even with $1/x^{3/2}$ singular structure functions.

The average transverse momenta in this scheme rise more strongly with energy than in previous versions of DTUJET. In hadronic collisions, we get a satisfactory phenomenology at the energies of the CERN and Tevatron colliders.

In order to get a consistent model using parton structure functions with Lipatov behavior, we have to introduce an energy-dependent transverse momentum cutoff for minijets. For nonsingular parton structure functions, the model is largely independent on this arbitrary cutoff.

ACKNOWLEDGMENTS

One of the authors (J.R.) acknowledges useful discussions with B. Andersson, V. N. Gribov, and A. B.

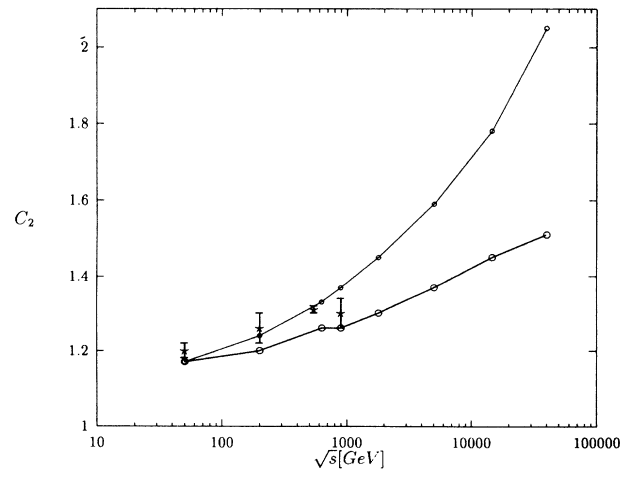

FIG. 29. Comparison of multiplicity moments with collider data [42,43]. The experimental data are with error bars, the upper curve is calculated with DTUJET92, the lower curve is calculated with DTUJET93.

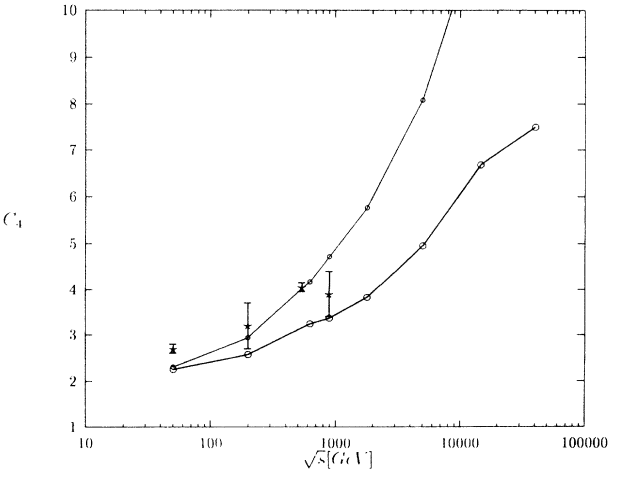

FIG. 31. Comparison of multiplicity moments with collider data [42,43]. The experimental data are with error bars, the upper curve is calculated with DTUJET92, the lower curve is calculated with DTUJET93.

Kaidalov. This work was started when one of the authors (J.R.) was at the Dept. of Theoretical Physics at Lund. He thanks Professor B. Andersson for the hospitality and support in Lund. One of the authors (R.E.) acknowledges the support by the Deutsche Forschungsgemeinschaft, Contract No. Ra 559/3-1.

[1] G. F. Chew and C. Rosenzweig, Nucl. Phys. **B104**, 290 (1976).
[2] C. Hong-Mo, J. E. Paton, and T. Sheung Tsun, Nucl. Phys. **B86**, 470 (1975).
[3] A. Capella, U. Sukhatme, C. I. Tan, and J. Tran Thanh Van, Phys. Rep. **236**, 227 (1994).
[4] A. Capella, J. Tran Thanh Van, and J. Kwiecinski, Phys. Rev. Lett. **58**, 2015 (1987).
[5] P. Aurenche, F. W. Bopp, A. Capella, J. Kwiecinski, M. Maire, J. Ranft, and J. Tran Thanh Van, Phys. Rev. D **45**, 92 (1992).
[6] F. W. Bopp, A. Capella, J. Ranft, and J. Tran Thanh Van, Z. Phys. C **51**, 99 (1991).
[7] F. W. Bopp, D. Pertermann, and J. Ranft, Z. Phys. C **54**, 683 (1992).
[8] R. Engel, F. W. Bopp, D. Pertermann, and J. Ranft, Phys. Rev. D **46**, 5192 (1992).
[9] S. Roesler, R. Engel, and J. Ranft, Z. Phys. C **59**, 481 (1993).
[10] B. L. Combridge, J. Kripfganz, and J. Ranft, Phys. Lett. **70B**, 234 (1977).
[11] I. Abt *et al.*, Nucl. Phys. **B407**, 515 (1993).
[12] J. Durand and H. Pi, Phys. Rev. Lett. **58**, 2015 (1987).
[13] X. N. Wang and M. Gyulassy, Phys. Rev. D **44**, 3501 (1991).
[14] K. Hahn and J. Ranft, Phys. Rev. D **41**, 1463 (1990).
[15] A. D. Martin, R. G. Roberts, and W. J. Stirling, Phys. Rev. D **47**, 867 (1993).
[16] C.-C. J. Botts *et al.*, Phys. Lett. B (to be published).
[17] E. M. Levin, in *QCD—20 Years Later,* Proceedings of the Workshop, Aachen, Germany, 1992, edited by P. M. Zerwas and H. A. Kastrup (World Scientific, Singapore, 1993).
[18] G. Arnison *et al.*, Phys. Lett. **128B**, 336 (1983).
[19] UA4 Collaboration, M. Bozzo *et al.*, Phys. Lett. **147B**, 392 (1984).
[20] N. A. Amos *et al.*, Nucl. Phys. **B262**, 689 (1985).
[21] UA4 Collaboration, D. Bernard *et al.*, Phys. Lett. B **198**, 583 (1987).
[22] UA5 Collaboration, G. J. Alner *et al.*, Z. Phys. C **32**, 153 (1986).
[23] E710 Collaboration, N. A. Amos *et al.*, Phys. Lett. B **243**, 158 (1990).
[24] G. J. Alner *et al.*, Phys. Rep. **154**, 247 (1987).
[25] UA4 Collaboration, D. Bernard *et al.*, Phys. Lett. B **186**, 227 (1987).
[26] J. C. M. Armitage *et al.*, Nucl. Phys. **B194**, 1365 (1982).
[27] UA5 Collaboration, R. E. Ansorge *et al.*, Z. Phys. C **33**, 175 (1986).
[28] UA1 Collaboration, D. Robinson, and C. E. Wulz, Report No. UA1-TN/89-10, 1989 (unpublished).
[29] E710 Collaboration, N. A. Amos *et al.*, Phys. Lett. B **301**, 313 (1993).
[30] M. Honda *et al.*, Phys. Rev. Lett. **70**, 525 (1993).
[31] Fly's Eye Collaboration, R. M. Baltrusaitis *et al.*, Phys. Rev. Lett. **52**, 1380 (1984).
[32] T. Sjöstrand, CERN Report No. CERN-TH.6488/92, 1992 (unpublished).
[33] J. Kwiecinski, A. D. Martin, R. G. Roberts, and W. J. Stirling, Phys. Rev. D **42**, 3645 (1990).
[34] K. Geiger, Phys. Rev. D **46**, 4965 (1992).
[35] K. Geiger, Phys. Rev. D **46**, 4986 (1992).
[36] K. Geiger, Phys. Rev. D **47**, 133 (1993).
[37] UA5 Collaboration, G. J. Alner *et al.*, Z. Phys. C **33**, 1 (1986).
[38] CDF Collaboration, F. Abe *et al.*, Phys. Rev. D **41**, 2330 (1990).
[39] C. Albajar *et al.*, Nucl. Phys. **B335**, 261 (1990).
[40] UA7 Collaboration, E. Pare *et al.*, Phys. Lett. B **242**, 531 (1990).
[41] T. Alexopolous, Phys. Rev. D **48**, 984 (1993).
[42] UA5 Collaboration, G. J. Alner *et al.*, Phys. Lett. **160B**, 193 (1985); **160B**, 199 (1985).
[43] R. E. Ansorge *et al.*, Z. Phys. C **43**, 357 (1989).